Flux jumps in ring-shaped and assembled bulk superconductors during pulsed field magnetization

Difan Zhou[1,2], Yunhua Shi[2], Anthony R Dennis[2], David A Cardwell[2] and John H Durrell[2]

1. Department of Physics, Shanghai University, Shanghai 200444, China
2. Department of Engineering, University of Cambridge, Trumpington Street, Cambridge CB2 1PZ, United Kingdom

Bulk (RE)BCO, where RE is a rare-earth element or yttrium, superconductors fabricated in the form of rings are potentially useful for a variety of solenoidal-type applications, such as small, high field NMR and electromagnetic undulators. It is anticipated that the practical exploitation of these technologically important materials will involve pulse field magnetization (PFM) and, consequently, it is important to understand the behavior of ring-shaped samples subjected to the PFM process. Macroscopic flux jumps were observed in PFM experiments on ring-shaped bulk samples when the peak applied field reaches a threshold magnitude, similar to behavior reported previously in cylindrical samples. Magnetic flux jumps inward when the thermal instability is triggered, however it subsequently flows outwards from the sample, resulting in a relatively low trapped field. This behavior is attributed to a variety of effects, including the inhomogeneity of material, which may lead to the formation of localized hot spots during the PFM process. In order to further elucidate this phenomena, the properties of a structure consisting of a bulk superconducting ring with a cylindrical superconductor core were studied. We observe that, although a flux jump occurs consistently in the ring, a critical state is established at the boundary of the ring-shaped sample and the core. We provide a detailed account of these experimental observations and provide an explanation in terms of the current understanding of the PFM process.

Introduction

Bulk superconductors have the ability to trap large magnetic field and may therefore be used potentially as cryo-permanent magnets. Durrell *et al*. reported a trapped field of 17.6 T at the centre of a stack of two $GdBa_2Cu_3O_{7-\delta}$ (GdBCO) bulk superconductors at 26 K, with 17.24 T having been achieved previously in an equivalent arrangement of $YBa_2Cu_3O_{7-\delta}$ (YBCO) [1, 2]. Ring-shaped (annular) bulk superconductors that enable access to these large magnetic fields have been investigated for various applications, such as compact NMR [3-10] and for more general applications [11-14]. However, *in-situ* magnetization on these materials remains a significant challenge and a barrier to practical applications of these technologically important materials. We have demonstrated previously that pulse field magnetization (PFM) is a promising experimental approach, and especially when flux jumps are exploited to assist the magnetic flux penetration in pre-cooled superconductors [15-17].

Flux jumps during PFM have been observed at a macroscopic scale in many studies [18-21]. These flux jumps occur when the applied pulsed magnetic field as well as its ramp rate (fixed pulse period) reaches a threshold magnitude [17], and manifest as a sudden increase in magnetic flux density within the sample. They are considered to be triggered by a thermomagnetic instability [22-26] induced by the pulsed magnetic field. Microscopic avalanches of vortices in $YBa_2Cu_3O_{7-\delta}$ (YBCO)

thin films have been observed to form dendrites using magneto-optical imaging [27, 28]. The morphology of these dendrites [29, 30] changes with ramp rate of the external magnetic field ($d\boldsymbol{B}_a/dt$) and operating temperature, which provides a general image of the nature of flux jumps. Dendritic flux jumps in thin films tend to be inhomogeneous and occur unpredictably. In addition, the tips can extend rather deep into the sample, making it difficult to define the penetration depth and hence the "size" of a particular flux jump. However, for bulk superconductors, flux jumps occur under predictable conditions during the PFM process. As a result, overall, it is possible to achieve a trapped field profile after PFM that is characterised by a single peak for a single grain bulk sample, as is obtained generally in a field-cooled (FC) process. The behavior of YBCO bulk superconductors differs significantly from that of thin films in at least three respects: the landscape and homogeneity of flux pinning sites, transient heat distribution and homogeneity of material (*e.g.* intrinsic grain boundaries and the presence of Y_2BaCuO_5 particles distribution due to push/trap effects), which may lead to different dynamical behavior of magnetic flux during a flux jump. Furthermore, at lower temperatures, flux jumps are prone to occur at the outer region of the bulk superconductor, which leads to two distinct and separated peaks in the trapped field profile. It is, therefore, essential to explore the region of avalanche instability and/or the "size" of flux jumps in the PFM process [31] in order to effectively exploit this effect. We have observed further that pre-placement of magnetic flux with a two-step PFM technique may reduce the generation of heat, and hence moderate the extent of the region of instabilities. This reflects partly how the frozen-in vortices affect the magnetization of bulk samples [32].

In this work, ring-shaped and assembled bulk GdBCO samples provide an approach for investigating the size of the flux jumps. The trapped field decreases dramatically when the magnetic flux penetrates entirely through the ring area in a flux jump, which means the region of avalanche instability is greater than the wall thickness of the ring. However, this can be avoided by inserting a cylindrical superconducting core inside the ring. The discontinuity in heat conduction at the ring/core boundary effectively terminates the avalanche instability, and hence leads to the re-establishment of the critical state.

Experimental details

Single grain GdBCO (with Ag) samples were prepared by the well-established top-seeded melt-growth (TSMG) processing technique. Significant effort has been made over the past thirty years to improve flux pinning as well as the homogeneity of this material [33, 34]. The buffer layer technique [35-39], which utilizes a disk of chemical composition engineered specifically to transmit the biaxial texture from the seed crystal to the pressed pre-form with a drilled hole, enables *in-situ* growth of ring-shaped GdBCO samples, as shown in figure 1 (details of this process will be reported elsewhere). This technique provides three configurations of samples: cylindrical, ring-shaped and assembled (ring-shaped and core), for the study of the PFM process. The outer and inner diameters of a ring-shaped sample after growth are approximately 30 mm and 12 mm, respectively, and the thickness is 12 mm.

Figure 1. A photograph of the single grain GdBCO ring-shaped sample and a 12 mm diameter single grain cylindrical (core) sample.

Figure 2 shows the sample assembly arrangement used in the experiments. The sample was cooled conductively using a cryocooler with a controllable temperature range of 15 K to room temperature. The pulsed field was generated by discharging a capacitor bank through a copper-wound solenoid coil. The rise and fall times of the pulsed field waveform were around 25 ms and 480 ms, respectively, as shown in figure 3. The peak value of applied field is proportional to the voltage applied to the capacitor bank (inset of figure 3), and hence can be controlled relatively straightforwardly. An array of 5 Hall sensors was placed on the top surface of the sample with a separation of 2.5 mm between each device and positioned from the center to the edge of the sample. The Hall sensors were used to monitor flux density during the entire PFM process with a sampling rate of 2000 Hz, and to record the final trapped magnetic field 15 minutes after application of the magnetizing field (i.e. when both the magnetic flux and temperature are considered to be stable).

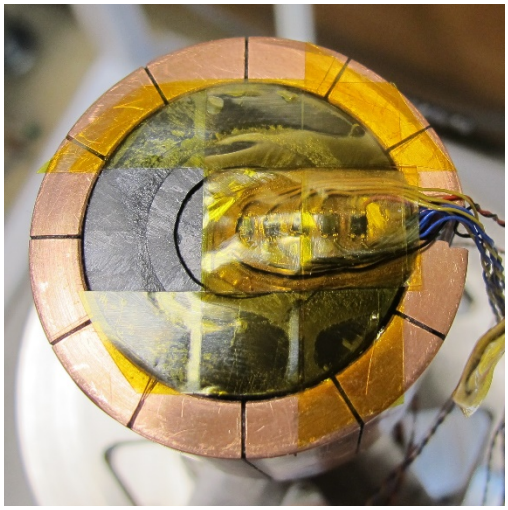

Figure 2. Sample assembly arrangement. Three Hall sensors are positioned on the inner core, and two sensors are on the ring. The distance between adjacent sensors is 2.5 mm. A further sensor is placed inside the bore of the ring.

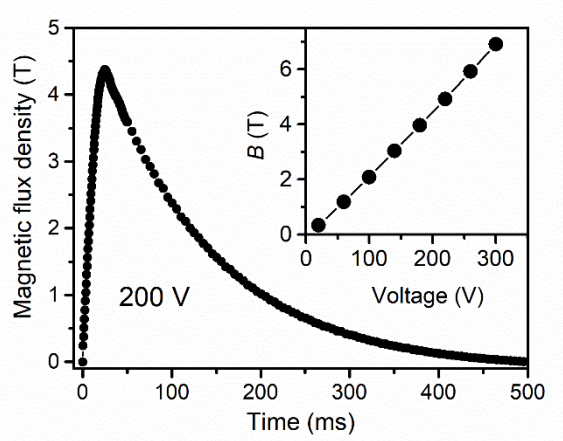

Figure 3. Waveform of the applied pulsed field for a set voltage on the capacitor bank of 200 V. The in-set shows the linear dependence of peak value of B_a on the set voltage.

A numerical simulation model that describes the penetration of magnetic flux into a ring-shaped sample was performed using a 2D model developed by Ainslie *et al* [40-43]. The general parameters used in the model are listed partly in table 1. This model was solved using Comsol commercial software.

Table 1. General settings of the 2D model

Governing equations	*H*-fomuation
E-*J* relationship	$E/E_c = (J/J_c)^n$, n = 21
$J_c(B, T)$	Experimental data for standard GdBCO sample measured by SQUID
Applied field (B_a)	Triangle wave with fixed ramp rate of 40 mT/s
Temperature	2D anisotropic heat thansient equtions using heat source of $Q = E \cdot J$

Results and Discussion

Figure 4 shows (a) the trapped field of a GdBCO ring-shaped and (b) the assembled sample. The samples were magnetized by the field cooling (FC) method in an applied field of 1.5 T at LN_2 temperature. The concentric distribution of trapped field observed for each sample arrangement indicates a relatively good material homogeneity. It can be seen that the field distribution remains uniform when the GdBCO core is inserted in the ring, and the peak value of trapped field reaches 1.1 T, which is a typical value for the 30 mm diameter bulk GdBCO samples. Note that the boundary of the ring and core can be still distinguished in the cross-section profile in figure 4(c) from the difference in the gradient of trapped field versus distance curve.

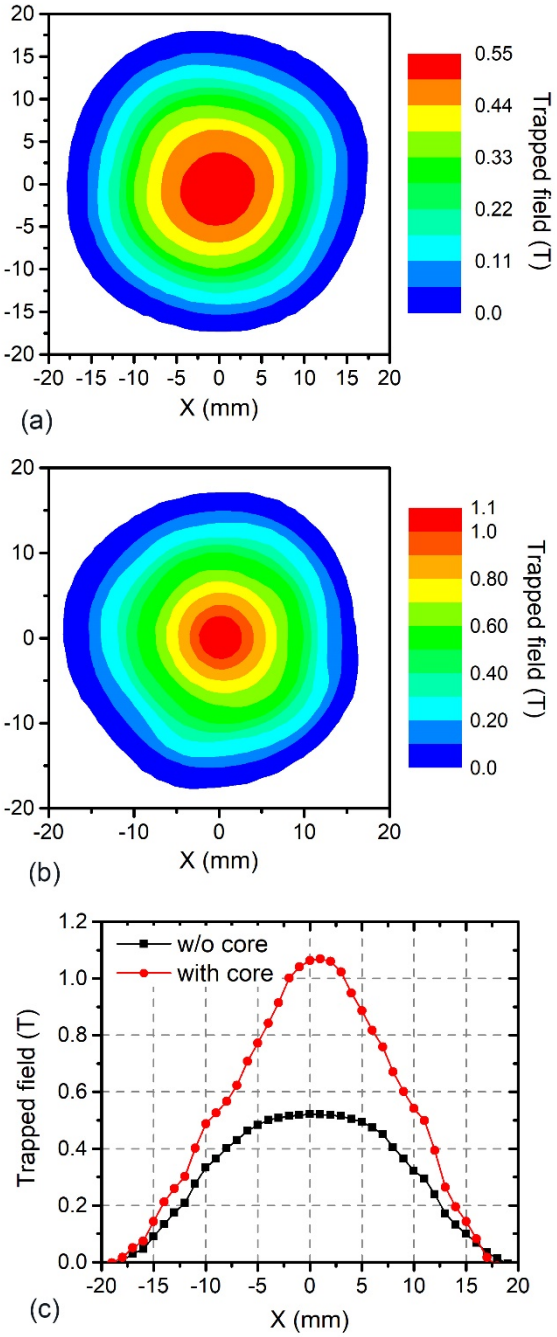

Figure 4 (a) Trapped field of the GdBCO ring-shaped and (b) assembled sample ring assembled sample obtained by field cooling magnetization. (c) The 1D trapped field profiles for the two sample arrangements.

The penetration of the magnetic field and resulting trapped field, according to Bean model under a quasi-static assumption for zero field cooling (ZFC), are illustrated schematically in figure 5. This is a 1D representation where $\mathrm{d}B/\mathrm{d}x = \mu_0 J$, which gives the dependence of penetration depth on the applied magnetic field (B_a). Here, we define the full penetration field, B_{fp}, as the value of applied field B_a that allows the magnetic flux or penetration front to reach the inner edge of the ring-shaped sample, and the full magnetisation field, B_{fm} as B_a that is required to fully magnetize the sample and

achieve the maximum trapped field.

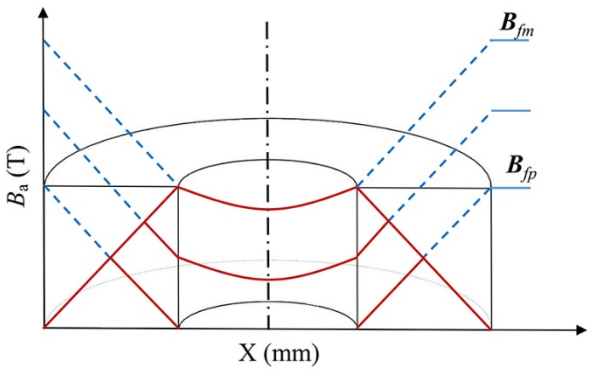

Figure 5. Schematic illustration of the critical state according to the Bean model in a ZFC process. B_{fp} and B_{fm} are the value of applied field required to fully penetrate and magnetize the sample, respectively.

Figure 6 shows the simulated trapped field profiles at the top-surface of the ring-shaped sample at 60 K and 30 K, which is consistent with the Bean model. It can be seen that B_{fp} and B_{fm} are approximately 2.5 T and 5 T at 60 K, and 8 T and 16 T at 30 K, respectively. Here, B_{fp} was determined when the shielding current was maximium and flowing throughout the sample cross section, as shown in figure 6(b). This model assumes a ramp rate B_a of 0.04 T/s, which constitutes a quasi-static ZFC process. The predicted temperature rise for an applied field B_a of 16 T at 30 K is less than 1.6 K.

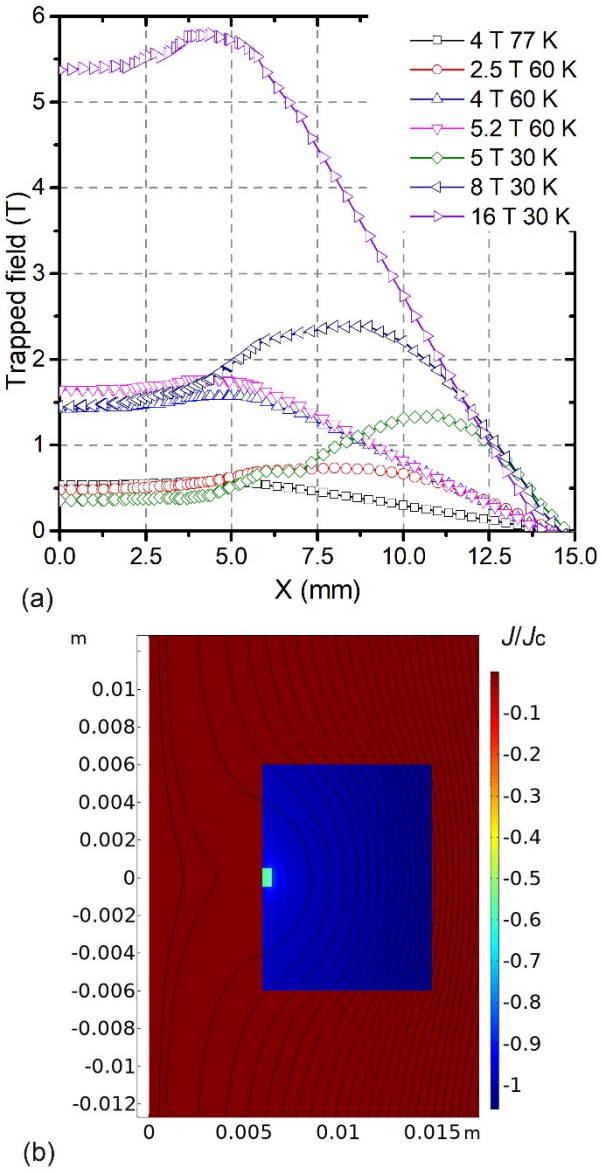

Figure 6 (a) Simulated trapped field at 60 K and 30 K for the ring-shaped sample and (b) the current density and stream lines through the sample cross section at 30 K for a background field of 8 T.

Figure 7 shows the resulting trapped field profiles of the ring-shaped sample after pulsed field magnetization at 60 K. This geometry enables a Hall sensor to be placed at the inner center of the sample to measure flux density (open symbols). The peak applied field, and hence the trapped field, was increased step-by-step for each measurement. It can be seen that the trapped field collapses partially when B_a reached 4.245 T (green curve with rhombohedral points). Furthermore, by careful comparison of the flux density at the center of the top-surface and inside the bore of the ring-shaped sample (indicated by red dashed square), it can be seen that magnetic flux is better shielded before B_a was increased to 4.01 T.

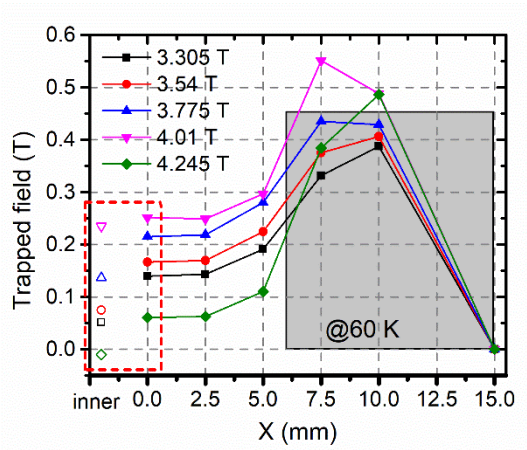

Figure 7. Resulting trapped field distribution at the top-surface and within the bore (open symbols) of the ring-shaped sample after PFM at 60 K. The grey-shaded, square area indicates the cross-section of the ring-shaped sample.

Figure 8 shows the variation of flux density recorded by the array of Hall sensors throughout the cross-section of the sample (i.e. from the center to the sample edge). It can be deduced from these data that the sample was shielded effectively by the induced current for B_a of 3.775 T, and that a flux jump occurred when B_a was increased to 4.01 T. These results are consistent with previous research that observed flux jumps are trigged when the applied field reaches a threshold value. The threshold B_a of 4.01 T (60 K) for the ring-shaped sample is close to that reported previously in [17] for a sample of cylindrical geometry.

The flux density inside the bore of the ring-shaped sample reaches a peak value of applied field after a slight delay in time following application of the pulse, as shown in figure 8 (b). However, magnetic flux then creeps out of the sample continuously. This is rather different from the behavior observed in a cylindrical sample, where, assisted by flux jumps, the magnetic flux penetrates inwards, and is immediately “frozen” in the sample [17]. A qualitative interpretation to above phenomena is that heat generated due to the movement of flux during the rise of B_a increases the sample temperature inhomogeneously from the outer region, thereby triggering the instability. At this moment, the “warm area” enters a resistive state and magnetic flux “jumps” into the sample until a critical state is re-established at the penetration front. In this case, a single peak, trapped field distribution similar to that characteristic of FC magnetisation can be achieved if the assumed penetration front is close to the center of the sample.

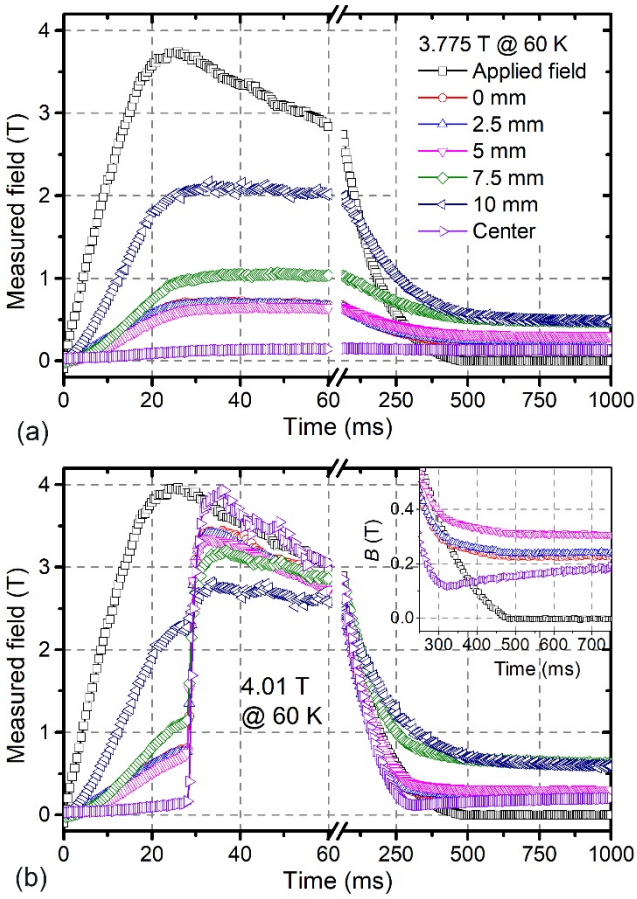

Figure 8 Variation of flux density measured for the ring-shaped sample at 60 K for an applied field B_a of (a) 3.775 T and (b) 4.01 T. The legend for (a) and (b) is the same.

If the "warm area" for a ring-shaped sample, is assumed to be greater than the thickness of the wall, the whole sample enters the resistive state and the magnetic flux may eventually flow out as B_a decreases. The inset of figure 8(b) shows that the flux density at the inner center of the sample first decreases to close to zero, and then increases when the applied field continues to decrease. We propose that the re-distribution of magnetic flux is driven by the local gradient of flux density due to the inhomogeneity of the material. As a result, hot spots will be generated and develop further into an "escape channel" for the magnetic flux. In this case, the distribution of trapped field will be *C*-shaped, as reported in [13] (a numerical simulation of this phenomenon will be reported by Fujishiro *et al*. elsewhere).

Figure 9 shows the resulting trapped field profiles of the assembled sample at 60 K, from which a flux jump is observed for a value of B_a of 3.775 T. This threshold value is slightly lower than that observed for the ring-shaped sample. Figure 10 shows the variation of flux density measured above the assembled sample. The third Hall sensor, located 5 mm away from the sample center, is at the edge of the core, as shown in figure 3. It can be seen that the flux jump occurs only within the region of the ring, and the core remains in a critical state during the entire PFM process. The interface between the ring and the core affects greatly the extent of thermal diffusion during the PFM process. The core remains cold after the ring has warmed up, and hence the critical state is rebuilt at the core-ring boundary when a flux jump occurs. It well supports our interpretation on the flux jumps that

the interface can be understood as an artificial penetration front.

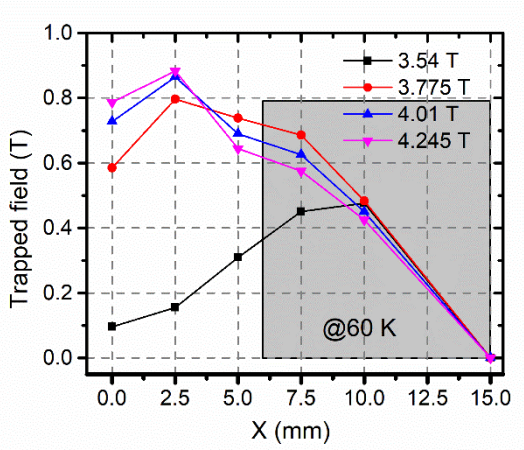

Figure 9 Trapped field of the assembly of a ring-shaped sample with a core insert at 60 K.

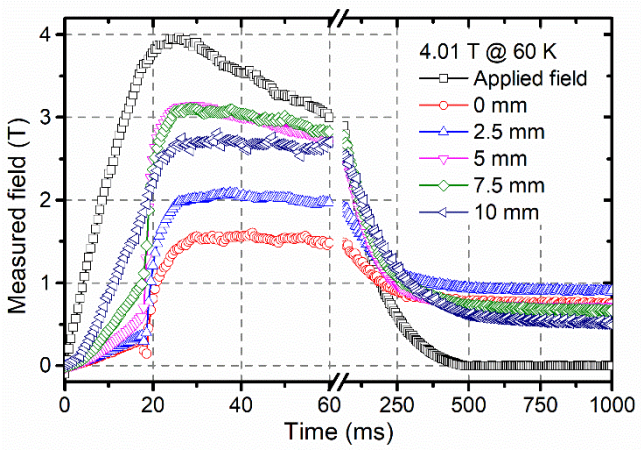

Figure 10 The evolution of magnetic flux density during a PFM process of the assembled sample for B_a of 4.01 T at 60 K.

Figure 11 compares the trapped field profiles of (a) the ring-shaped sample and (b) the assembled sample at 30 K after PFM. Figure 12 shows the evolution of flux density during the entire PFM process for B_a of 4.95 T, which is the threshold field to trigger a flux jump in the ring-shaped sample at 30 K. The flux density at the inner center decreases to zero when the applied field exceeds 5 T, as shown in figure 11(a), suggesting that “escape channels” for the flux have formed in the ring-shaped sample.

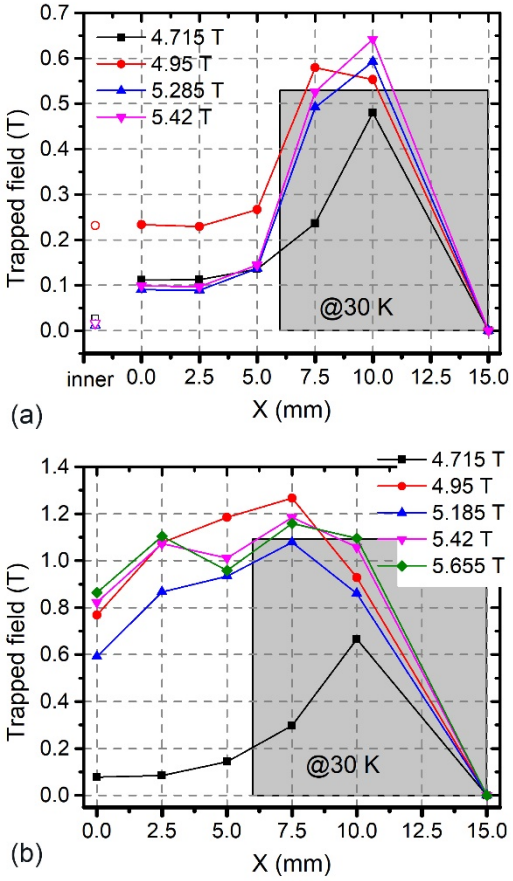

Figure 11 Trapped field profiles of (a) the ring-shaped sample and (b) the assembled sample after PFM at 30 K.

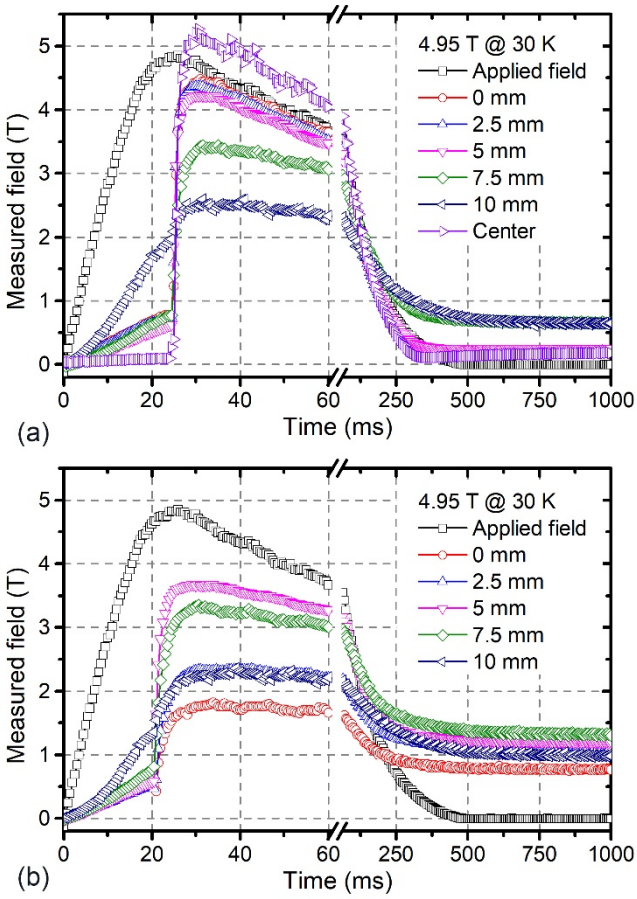

Figure 12 Comparison of flux density evolution during PFM between the (a) ring-shaped sample and (b) sample assembly when B_a of 4.95 T was applied at 30 K.

In general, the dynamical behavior of the magnetic flux at 30 K is similar to that observed at 60 K. However, J_c is significantly higher at 30 K than at 60 K, and hence B_{fp} should also be much higher (8 T at 30 K compared to 2.5 T at 60 K, according to the simulation). Therefore, a much shorter penetration depth is anticipated at 30 K, which means the flux jumps are more likely to occur at the outer portion of the sample. This can be inferred by comparing the trapped field profiles in figures 7 and 11(a). The intention was to achieve a critical state immediately after the occurrence of a flux jump within the ring-shaped sample, and therefore inhibit flux flow, by increasing B_a step-by-step with small intervals. However, it can be seen in figure 11(a), by comparing the flux density at the inner center for B_a of 4.95 T and 5.285 T, B_a of 4.95 T is already a rather critical value. The "warm area", or the size of flux jump, is presumably greater than the wall thickness of the ring for B_a of 4.95 T at 30 K.

Conclusions

The pulsed field magnetization of a superconducting GdBCO ring has been compared with that of rings assembled with a superconducting, cylindrical core. Flux jumps have been observed during the PFM process for both ring-shaped samples and assembled samples. The threshold applied field, B_a, required to trigger a flux jump instability is observed to be consistent with that reported previously for cylindrical samples. The boundary between the ring and core in the assembled sample affects the thermal diffusion, and the critical state is rebuilt naturally at this boundary. This

observation supports the understanding of the role and behavior of flux jumps in the PFM process. The re-establishment of the critical state immediately after a flux jump is considered critical to achieving a sufficiently high and FC-like trapped field, as has been observed in cylindrical samples. For the ring-shaped samples, however, magnetic flux jumps in once an instability is triggered and flows out subsequently, resulting in a relatively low trapped field. The critical state is not restored within the ring-shaped sample following a flux jump, and hence the redistribution of magnetic flux, driven by the local spatial gradient of magnetic flux density, cannot be prevented, and this may eventually lead to the formation of escape channels for magnetic flux. This effect may be attributed to inhomogeneity within the superconducting material or to the random nature of a flux jump, which is consistent with evidence provided by magneto-optical imaging. The combination of these effects is to make PFM of ring-shaped samples a much more challenging task than the application of this technologically important technique to solid cylindrical bulk samples.

Acknowledgement

This work was supported by the Engineering and Physical Sciences Research Council (grant number: EP/P00962X/1) and the State Key Laboratory of Traction Power at Southwest Jiaotong University (TPL-1709).

References

[1] J. H. Durrell, A. R. Dennis, J. Jaroszynski, M. D. Ainslie, K. G. B. Palmer, Y. Shi, A. M. Campbell, J. Hull, M. Strasik, E. E. Hellstrom and D. A. Cardwell, Supercond. Sci. Technol. **27**, 082001 (2014).

[2] M. Tomita and M. Murakami, Nature **421**, 517–20 (2003).

[3] K. Ogawa, T. Nakamura, Y. Terada, K. Kose and T. Haishi, Appl. Phys. Lett. **98**, 234101 (2011).

[4] T. Nakamura, D. Tamada, Y. Yanagi, Y. Itoh, T. Nemoto, H. Utumi and K. Kose, J. Mag. Reson. **259**, 68-75 (2015).

[5] Y. Iwasa, J. Bascuñán, S. Hahn, M. Tomita and W. Yao, IEEE Trans. Appl. Supercond. **20**, 718 (2010).

[6] S. Kim, S. Fukada, R. Nomura and H. Ueda, IEEE Trans. Appl. Supercond. **28**, 4301505 (2018).

[7] H. Fujishiro, Y. Itoh, Y. Yanagi and T. Nakamura, Supercond. Sci. Technol. **28**, 095018 (2015).

[8] J. H. Durrell, M. D. Ainslie, D. Zhou, P. Vanderbemden, T. Bradshaw, S. Speller, M. Filipenko and D. A. Cardwell, Supercond. Sci. Technol. **31**, 103501 (2018).

[9] W. Yang, D. Liao, Y. Ji and L. Yao. J. Appl. Phys., **124**, 213901 (2018)

[10] W. Yang, Y Ji, L. Yu, X. Liu, J Long, Z. Liu and D. Song, Supercond. Sci. Technol., **33**, 014001 (2020)

[11] H. Ohsaki, T. Shimosaki and N. Nozawa, Supercond. Sci. Technol. **15**, 754-758 (2002)

[12] Y. Komi, M. Sekino and H. Ohsaki, Physica C **469**, 1262-1265 (2009)

[13] H. Mochizuki, H. Fujishiro, T. Naito, Y. Itoh, Y. Yanagi, and T. Nakamura, IEEE Trans. Appl. Supercond. **26**, 6800205 (2016)

[14] M. Sander and M. Klaeser, IEEE Trans. Appl. Supercond. **11**, 3732-3735 (2001)

[15] D. Zhou, M. D. Ainslie, Y. Shi, A. R. Dennis, K. Huang, J. R. Hull, D. A. Cardwell, and J. H. Durrell, Appl. Phys. Lett. **110**, 062601 (2017).

[16] M. D. Ainslie, D. Zhou, H. Fujishiro, K. Takahashi, Y. Shi, and J. Durrell, Supercond. Sci. Technol. **29**, 124004 (2016).

[17] D. Zhou, M. D. Ainslie, Jan Srpčič, K. Huang, Y. Shi, A. R. Dennis, D. A. Cardwell, J. H. Durrell, M. Boll and M. Filipenko, Supercond. Sci. Technol. **31**, 105005 (2018).

[18] R. Weinstein, D. Parks, R-P. Sawh, K. Carpenter and K. Davey, Appl. Phys. Lett. **107**, 152601 (2015).

[19] H. Fujishiro, T. Tateiwa, A. Fujiwara, T. Oka, and H. Hayashi, Physica C 445, 334 (2006).

[20] Y. Yanagi, Y. Itoh, M. Yoshikawa, T. Oka, and U. Mizutani, Supercond. Sci. Technol. 18, 839 (2005).

[21] Y. Itoh, Y. Yanagi and U. Mizutani, J. Appl. Phys. **82**, 5600 (1997).

[22] S. L. Wipf, Cryogenics, **31**, 936 (1991).

[23] S. L. Wipf, Phys. Rev. **161**, 404 (1967).

[24] P. S. Swartz and C. P. Bean, J. Appl. Phys. **39**, 4991 (1968).

[25] K.-H. Müller and C. Andrikidis, Phys. Rev. B **49**, 1294 (1994).

[26] R. Mints, Phys. Rev. B **53**, 12311 (1996).

[27] E. Baruch-El, M. Baziljevich, B. Ya. Shapiro, T. H. Johansen, A. Shaulov and Y. Yeshurun, Phys. Rev. B **94**, 054509 (2016)

[28] P. Leiderer, J. Boneberg, P. Brüll, V. Bujok and S. Herminghaus, Phys. Rev. Lett. **71**, 2646 (1993).

[29] E. Altshuler and T. H. Johansen, Rev. Mod. Phys. **76**, 471 (2004).

[30] J. I. Vestgården, T. H. Johansen and Y. M. Galperin, L. Temp. Phys. **44**, 460 (2018).

[31] D. V. Shantsev, A. V. Bobyl, Y. M. Galperin, T. H. Johansen, and S. I. Lee, Phys. Rev. B **72**, 024541 (2005).

[32] F. Colauto, D. Carmo, A. M. H. de Andrade, A. A. M. Oliveira, W. A. Ortiz, and T. H. Johansen, Phys. Rev. B **96**, 060506 (2017).

[33] Y. Shi, D. K. Namburi, W. Zhao, J. H. Durrell, A. R. Dennis, and D. A. Cardwell, Supercond. Sci. Technol. **29**, 015010 (2016).

[34] D. Zhou, S. Hara, B. Li, K. Xu, J. Noudem, and M. Izumi, Supercond. Sci. Technol. **26**, 015003 (2013).

[35] Y. Shi, D. K. Namburi, W. Zhao, J. H. Durrell, A. R. Dennis, and D. A. Cardwell, Supercond. Sci. Technol. **29**, 015010 (2016)

[36] D. K. Namburi, Y. Shi, W. Zhai, A. R. Dennis, J. H. Durrell, D. A. Cardwell, Crystal Growth & Design **15**, 1472-1480 (2015)

[37] T. Li, L. Cheng, S. Yan, L. Sun, X. Yao, Y. Yoshida and H. Ikuta, Supercond. Sci. Technol. **23**, 125002 (2010)

[38] C. Kim, J. Lee, S. Park, B. Jun, S. Han and Y. Han, Supercond. Sci. Technol. **24**, 015008 (2011)

[39] D. Zhou, K. Xu, S. Hara, B. Li, Z. Deng, K. Tsuzuki and M. Izumi, Sci. Technol. **25**, 025022 (2012)

[40] M. D. Ainslie and H. Fujishiro, Supercond. Sci. Technol. **28**, 053002 (2015).

[41] M. D. Ainslie, H. Fujishiro, H. Mochizuki, K. Takahashi, Y. Shi, D. K. Namubri, J. Zou, D. Zhou, A. R. Dennis and D. A. Cardwell, Supercond. Sci. Technol. **29** 074003 (2016)

[42] M. D. Ainslie, J. Zou, H. Mochizuki, H. Fujishiro, Y. Shi, A. R. Dennis and D. A. Cardwell, Supercond. Sci. Technol. **28** 125002 (2015)

[43] M. D. Ainslie, H. Fujishiro, T. Ujiie, J. Zou, A. R. Dennis, Y. Shi and D. A. Cardwell, Supercond. Sci. Technol. **27** 065008 (2014)